Theor Chim Acta (1994) 88: 325–338

Theoretica Chimica Acta

Ab initio electronic analysis of the hydride transfer in the $[CH_3–H–CH_3]^+$ system

J. Mestres[1,2], M. Duran[1], J. Bertrán[2]

[1] Institut de Química Computacional, Departament de Química, Universitat de Girona, Plaça de l'Hospital 6, E-17071 Girona, Catalonia (Spain) [2] Grup de Química Teòrica, Departament de Química, Universitat Autònoma de Barcelona, E-08193 Bellaterra, Catalonia (Spain)

Received June 6, 1993/Accepted October 10, 1993

Summary. The electronic aspects of the hydride transfer process between CH_4 and CH_3^+ fragments, are studied theoretically with *ab initio* molecular orbital methods, subject to the constraint of maintaining a fix distance between both fragments. Mulliken and Natural population analyses are performed to gain an insight into the hydride character of the atom being transferred. From these analyses, charge migrating diagrams are depicted to obtain a more visual information. Further analysis is performed from the contour maps of the electronic charge density, together with the analysis of its gradient and laplacian. Basis set and electronic correlation effects are also discussed. Finally, the effect of applying a uniform electric field is assessed.

Key words: Hydride transfer – $C_2H_7^+$ system – Charge population analysis – Charge migrating diagrams – Electron density contour maps

1 Introduction

The nature of the transferring H in formally-termed hydride transfer processes has been a matter of controversy since 1955, when Mauzerall and Westheimer [1] published the first mechanistic study on such processes. This study opened an active area of investigation in the elucidation of the mechanistic details of this kind of reactions: are they really concerted one-step hydride transfer processes or must one take into account multi-step mechanisms involving a single electron transfer (SET) step? Furthermore, even considering the hypothesis of a concerted one-step pathway, this controversy can be extended when thinking on the timing of the electronic reorganisation: is the transferring H a real hydride or does an inner-sphere electron transfer mechanism have to be considered to reflect the coupling between the H motion and the electronic shift?

In regard to the literature on this subject, hydride transfer processes could be clearly divided into two groups, namely non-enzymic and enzymic hydride transfers, the main difference between them being the distance to be covered by the transferring H: in non-enzymic hydride transfers there is a large variation in the

distance between the heteroatoms involved in the H-transfer when going from reactants to transition state, while in enzymic hydride transfers there are some special environmental constraints that practically fix this distance throughout the process. A huge number of both experimental and theoretical works on both type of hydride transfers have appeared in the last four decades. Experimentalists have tried to mimic enzymic hydride transfers by nonenzymic hydride processes [2, 3], in which simple 1,4-dihydronicotinamides act as hydride donors towards suitable acceptor molecules. However, this model does not take into account that constraints existing inside the active site of enzymes provide special characteristics to this type of hydride transfers, as mentioned above. As a matter of fact, a noteworthy experimental effort has been done to model these particular enzymic conditions by crown ether complexes [4]. Further, Dewar and Storch [5] pointed out that adsorption of the substrate into the active site of the enzyme can occur if all molecules of solvent (i.e., water) are squeezed out from between them, so one can consider that the enzymic reaction proceeds in the absence of solvent, in a manner analogous to a reaction in the gas phase. As a consequence, they stated that since gas-phase reactions often differ dramatically from analogous reactions in solution, discussions on enzymic reactions should be based indeed on analogies with gas-phase processes. This is the reason why enzymic processes have been frequently modelled, at a theoretical level, as reactions between gas-phase reactant analogues through addition of several geometrical constraints in the calculation, according to available experimental information on the active site of the enzyme [6]. One step forward involves including the effect of the proteinic environment in these theoretical treatments. For that purpose, several attempts have been done by including a reaction field [6(d)] or a uniform electric field [7] in the gas-phase calculations, and by analyzing the role of the environment in the catalytic activity of enzymes [8].

Despite this subject having been regarded from all these points of view, the H-transfer event, and in fact the nature of the transferring H itself, is not completely clear yet. In this paper we have studied the simplest model system, namely the gas-phase $CH_4 + CH_3^+ \rightarrow CH_3^+ + CH_4$ reaction, where a formal hydride transfer between two carbons, subject to the constraint of fixing the distance between them, can take place. In this sense we will treat an enzymic-like hydride transfer process. A previous study [7] showed that, in these conditions, the H-transfer event in this system evolves in a concerted one-step pathway. However, it would be interesting to clarify the timing of the electronic reorganisation in these concerted pathways in order to obtain a deeper insight in the accumulation of the charge density around the H being transferred. This has been the aim of this paper. Further, in a second step, the electric field created by the enzymic environment has been modelled in some manner by the application of a uniform electric field along the C–H–C axis.

2 Methodology

This theoretical investigation has been executed by means of *ab initio* molecular orbital calculations at the SCF, CASSCF, MP2 and CISD levels of theory using the 6-31G** basis set [9]. CASSCF calculations have been performed taking as the active space the two electrons and the three orbitals being involved in the transfer event, namely one occupied (bonding) and two virtual (nonbonding and antibonding). Restricted geometry optimizations have been accomplished through the method owing to Schlegel [10]. Natural population (NPA) and natural bond orbital (NBO) analyses have been done by the method of Weinhold et al. [11]. All

calculations have been made using the Gaussian 90 program [12]. Electron density and gradient contour maps have been examined according to Bader analyses [13]. The effect of an external uniform electric field has been included by adding the electron-field interaction term into the one-electron Hamiltonian.

3 Results and discussion

This work deals with the linear hydride transfer in the $[CH_3–H–CH_3]^+$ system. The geometries of the reactant complex (RC) and the product complex (PC) have been restricted to have a C_{3v} symmetry, while that of the transition state (TS) has been restricted to have a D_{3d} symmetry. This notwithstanding, we have checked that unrestricted geometry optimization calculations, starting from unsymmetric geometries, converge towards symmetry-restricted geometries. To model an enzymic-like process, we have fixed the value of C–C distance between the CH_4 and the CH_3^+ fragments to 3.2 Å (Scheme I). This value has been taken according to various experiments showing that the separation of the atoms between which the hydrogen atom is exchanged lies within a range of 2.7–3.5 Å. For instance, Sustmann et al. [14] found a separation of 3.2 Å in his X-ray study on the structure of glutathione reductase.

From now on, we present first the results for the gas-phase reaction, and second, the results obtained when a uniform electric field along the C–H–C axis is applied.

3.1 Gas-phase reaction

In Table 1 we have collected the geometrical parameters according to Scheme I, together with the energies and the energy barriers for the four different levels of theory employed. The parameters for PC are omitted because of the symmetry of the process.

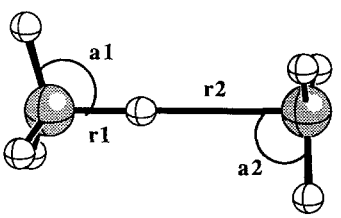

Scheme I

Taking an insight into the geometrical parameters, one can observe that the $r1$ value reflects clearly the polarization effect of the CH_3^+ fragment on the C–H_t bond of the RC (H_t stands for the H being transferred). This value is always larger than that for the other terminal C–H bonds of the CH_4 fragment (ca. 1.08 Å). Moreover, $r1$ depends clearly on the level of theory being used: inclusion of electron correlation effects increases its value due to the fact that the antibonding orbital is allowed to participate in the electronic wavefunction; this factor translates into a lower occupation number for the bonding orbital and a lengthening of the C–H_t bond. In a valence bond language, one might say that ionic structures are less exaggerated if

Table 1. Geometrical parameters (in Å), energies (in hartrees), and energy barriers (in kcal/mol) for the reactant complex and the transition state using the four different theoretical levels employed

Level	Point	$r1$	$r2$	$a1$	$a2$	E	ΔE
SCF	RC	1.1240	2.0760	107.38	91.17	−79.44768	
	TS	1.6		97.54		−79.42588	13.68
CASSCF	RC	1.1553	2.0447	106.74	91.54	−79.47164	
	TS	1.6		97.84		−79.45827	8.39
MP2	RC	1.1500	2.0500	106.38	91.65	−79.72979	
	TS	1.6		97.53		−79.71666	8.24
CISD	RC	1.1404	2.0596	106.74	91.44	−79.76887	
	TS	1.6		97.52		−79.75655	7.73

correlation energy is accounted for. In turn $r2$ is defined simply as the difference between the fixed C–C distance (3.2 Å) and $r1$; in TS, $r1$ and $r2$ have always a value of 1.6 Å. Besides the most important motion of this process, i.e., the transfer of H_t, another motion appears in the terminal hydrogens when going from RC to TS and to PC, due to the change occurring in the hybridization character of the two carbon atoms. For instance, the hybridization of carbon in the CH_4 fragment switches from sp^3 to sp^2, which is revealed by the values for the $a1$ and $a2$ angles. Thus, in RC $a1$ is significantly larger than $a2$; in TS, their values become similar. It is worth noting that no important differences have been obtained for these angle values comparing the four levels of calculation employed.

Energies of RC and TS are also gathered in Table 1; those at the CISD level of calculation include the Davidson size-consistency correction to estimate the effect of quadruple excitations. Looking at the values of the energetic barriers, one can see that when electron correlation is included, the barrier is fairly lowered, reflecting the fact that TS is more stabilized than RC. In average, this process features a barrier of ca. 10 kcal/mol, which is small enough to be considered as realistic for enzymic-like processes. It is convenient to emphasize that at all levels of theory considered, the shape of the potential energy profile reflects a concerted one-step process.

In order to obtain a first insight into the electronic character of H_t, two kinds of population analyses have been done, namely the Mulliken (MPA) and the natural (NPA) population analyses. The latter has recently emerged as a powerful alternative to the former [11]: not only does NPA share with MPA a low computing cost, but also it seems to overcome basis set dependence, which is one of the most serious limitations of MPA. The various analyses have been performed using the one-electron density matrices corresponding to each level of calculation used: for SCF calculations the SCF density has been taken; for MP2 calculation, we have used the generalized density corresponding to the second-order energy; and for CISD and CASSCF calculations the generalized density corresponding to the CI energy has been employed. MPA analyses have been done on all four cases, while only the SCF and the MP2 densities have been taken for the NPA analyses as comparison to MPA.

In Tables 2 and 3 we have collected the fragment charges obtained from the respective MPA and NPA analyses. We have considered that the reaction proceeds from left to right, that is, the H being transferred (H_t) is initially bonded to the CH_3

Table 2. Mulliken population analyses by fragments using the SCF, MP2 and CI one-electron density matrices according to the level of theory employed

Level	Fragment	RC	TS	PC	ΔQ
SCF	H_1	−0.0881	−0.1776	−0.0881	−0.0895
	CH_3^{ℓ}	0.1666	0.5888	0.9215	0.4222
	CH_3^{r}	0.9215	0.5888	0.1666	−0.3327
	Q_{trans}	−0.0785	−0.4112	−0.8334	−0.7549
CASSCF	H_t	−0.0945	−0.0604	−0.0945	0.0341
	CH_3^{ℓ}	0.1984	0.5302	0.8961	0.3318
	CH_3^{r}	0.8961	0.5302	0.1984	−0.3659
	Q_{trans}	−0.1039	−0.4698	−0.8016	−0.6977
MP2	H_t	−0.0540	−0.0318	−0.0540	0.0222
	CH_3^{ℓ}	0.1876	0.5159	0.8664	0.3283
	CH_3	0.8664	0.5159	0.1876	−0.3505
	Q_{trans}	−0.1336	−0.4841	−0.8124	−0.6788
CISD	H_t	−0.0702	−0.0786	−0.0702	−0.0084
	CH_3^{ℓ}	0.1831	0.5393	0.8871	0.3562
	CH_3^{r}	0.8871	0.5393	0.1831	−0.3478
	Q_{trans}	−0.1129	−0.4607	−0.8169	−0.7040

Table 3. Natural population analyses by fragments using the SCF and MP2 density matrices

Level	Fragment	RC	TS	PC	ΔQ
SCF	H_t	0.0796	−0.0850	0.0796	−0.1646
	CH_3^{ℓ}	−0.0101	0.5425	0.9305	0.5526
	CH_3^{r}	0.9305	0.5425	−0.0101	−0.3880
	Q_{trans}	−0.0695	−0.4575	−1.0101	−0.9406
MP2	H_t	0.1013	0.0472	0.1013	−0.0541
	CH_3^{ℓ}	0.0225	0.4764	0.8762	0.4539
	CH_3^{r}	0.8762	0.4764	0.0225	−0.3998
	Q_{trans}	−0.1238	−0.5236	−0.9775	−0.8537

fragment on the left (CH_3^{ℓ}), and evolves towards the CH_3 fragment on the right (CH_3^{r}). With this assumption, ΔQ may be defined as the difference in charge that each fragment experiences when going from RC to TS; the parameter Q_{trans} is added on each bottom line to provide an idea of the charge that has been transferred to CH_3^{r}, taking as a reference a + 1 charge on CH_3^{r} at infinite separation. In this way, the lower-right-corner value at each level of analysis turns out to be the effective total charge transferred to CH_3^{r}.

Paying attention to Table 2, at first glance the most striking result is that the charge on H_t in TS is only scarcely negative at all levels of theory used: comparing the value obtained for each level of calculation, the SCF and MP2 levels furnish, respectively, the most negative and the most positive charges on H_t. Moreover, when the reaction proceeds from RC to TS, only at the SCF level does H_t becomes clearly a little more negative. At the CISD level, there is almost no change in charge along the reaction coordinate, whereas at the MP2 and CASSCF levels this change

is slightly positive. Furthermore, we have tested, at the SCF level, the effect of adding a diffuse function on H_t in order to allow for more concentration of electronic charge on H_t if this is favourable. The fragment charges in RC on H_t, CH_3^l and CH_3^r are, respectively, −0.0948, 0.1800 and 0.9148 au, while in TS become −0.1674, 0.5837 and 0.5837 a.u. As can be seen, the results obtained do not substantially differ from those obtained at the SCF level with the 6-31G** basis set (Table 2).

Thus, from these results it is difficult to state that a real hydride is moving from one CH_3 fragment to the other. Another interesting point is that the charge on the two CH_3 fragments changes dramatically when going from RC to TS. These two facts allow to introduce the idea that the process seems to seek an inner-sphere electron transfer mechanism, i.e., some charge density is being transferred further the H-atom position.

In Table 3 the results of the NPA analyses at the SCF and MP2 levels (taken as the two limiting cases) are shown. The analyses conducted here can test the reliability of MPA atomic charges because we have used a large basis set. There are two interesting points to comment out: first, comparing the two analyses at the same levels of theory, one can see that NPA analyses give significantly less negative atomic charges on H_t than MPA do. Furthermore, this effect is larger on RC that on TS, thus translating into a higher change in the charge of H_t when the reaction advances; second, NPA analyses show the same trend of MPA analyses when comparing the results for the different levels of calculation performed.

In summary, the results obtained from the two population analyses do not differ substantially, and thus both results seem equally good. In this sense, one can compare the relative results of the two population analyses on the four levels of theory employed, by dividing the change in charge undergone by the CH_3^r fragment by the total effective charge transferred in the process. In all eight cases, the value obtained is close to 50% of charge transferred, which reinforces the above conclusion on the existence of an inner-sphere electron transfer mechanism.

In order to provide a more visual picture of the change in charges undergone by the different fragments during the process, charge migration diagrams can be constructed in a qualitative way by connecting the results obtained from RC, TS, and PC in Table 2. In Fig. 1 we have depicted the SCF (solid lines) and MP2 (dashed lines) values obtained from the Mulliken population analyses; these two

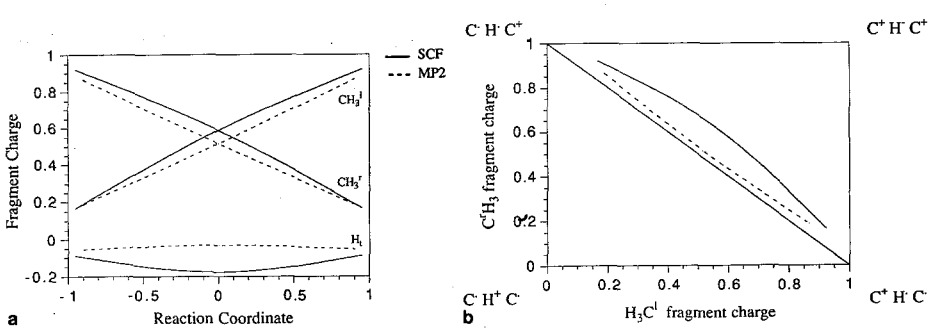

Fig. 1a, b. Charge migrating diagrams: reaction coordinate vs. fragment charge diagram (**a**) and valence bond structure-related diagram (**b**). Solid lines stand for SCF level and dashed lines for MP2 level

levels of calculation are chosen as limiting cases. Such diagrams have been already used in earlier works dealing with hydride transfers [2(c), 3(b), 3(f)] to define the degree of advance in a charge-change sense.

Figure 1a describes the change in charge of the fragments along the reaction coordinate q, which is defined as the difference between $r1$ and $r2$. As can be observed, a weak change in charge is found for H_t, while the charges of the two CH_3 fragments undergo a noticeable change.

Figure 1b furnishes the same fragment charge information, yet relating it to the four meaningful valence bond structures involved in a formal hydride transfer, namely $C^{\cdot}H^{\cdot}C^{+}$, $C^{+}H^{\cdot}C^{\cdot}$, $C^{+}H^{-}C^{+}$, and $C^{\cdot}H^{+}C^{\cdot}$. The reactant and product complexes (represented by the $C^{\cdot}H^{\cdot}C^{+}$ and $C^{+}H^{\cdot}C^{\cdot}$ structures) are located at the upper-left corner and the lower-right corner, respectively. The upper-right corner and the lower-left corner correspond to two limiting cases of the transition state, i.e., the $C^{+}H^{-}C^{+}$ structure, representing a pure hydride character, and the $C^{\cdot}H^{+}C^{\cdot}$ structure, being related to a pure proton character. Thus, the abcissa and the ordinate represent the change in charge of the hydride donor and the hydride acceptor species, respectively, varying from 0 to +1. Moreover, the diagonal linking the upper-left and the lower-right corners denotes a value of 0 for the atomic charge on H_t. Lines above indicate an increase in the hydride character of H_t, while lines below symbolize that a proton character is emerging. Thus, Fig. 1b discloses that the paths calculated at the two levels of calculation follow closely the main diagonal, mirroring the weak change in charge of the H_t, together with the important change in charge of the two CH_3 fragments.

We have also carried out a natural bond orbital (NBO) analysis at the SCF and MP2 levels of theory from the respective one-electron density matrices. When performing this type of analysis, we have allowed for the existence of strongly delocalized natural bond orbitals, and hence searched for three-center bonds.

In the NBO method the bonding in each species is characterized by spatially directed hybrids on each center. The percentages of natural hybrid s, p and d character of each bonding NBO for the transition state are gathered in Table 4, together with the polarization coefficients of each bond, i.e., the contribution of the hybrid on each center to the total bond. This table reveals that a strongly delocalized structure (denoted as a three-center orbital C^{ℓ}–H_t–C^{r}) has been found for each level of theory. This orbital becomes composed by the s-character hybrid

Table 4. Natural bond orbital analysis at the SCF and MP2 levels

Level of theory	Bond	Center	% hybrid s character	% hybrid p character	% hybrid d character	Polarization coefficient
SCF	C^{ℓ}–H_t–C^{r}	C^{ℓ}	3.21	96.63	0.16	0.4785
		H_t	100.00			0.7362
		C^{r}	3.21	96.63	0.16	0.4785
	C–H	C	32.20	67.64	0.16	0.7958
		H	99.85	0.15		0.6055
MP2	C^{ℓ}–H_t–C^{r}	C^{ℓ}	2.96	96.90	0.14	0.5089
		H_t	100.00			0.6942
		C^{r}	2.96	96.90	0.14	0.5089
	C–H	C	32.30	67.56	0.14	0.7966
		H	99.88	0.12		0.6046

of the H_t and the *p*-character hybrid of each C center, formed exclusively by the *p* orbitals directed along the C–H–C axis. For the sake of comparison, we have added the hybridization percentages of one of the six other bonding orbitals arising from the six symmetry-alike C–H terminal bonds. From these values one can observe that the hybridization of the C atom is almost perfectly sp^2.

Bond polarization coefficients appear to follow simple electronegativity relations, as more covalent bonds are formed between atoms of similar electronegativity. The relative magnitudes of these coefficients among centers indicate the covalency of the bond. In this sense, the C–H terminal bonds show a typical covalent bond, the polarization coefficient on the C center being higher than that on the H center, following the electronegativity scale. As can be noticed, the three-center bond exhibits clearly a smaller covalent character: now, an inversion in the magnitude of the polarization coefficient of each center has occurred (the polarization coefficient on the H_t center is noticeably larger, especially at the SCF level, than those on the C centers); furthermore, the relative difference between the two values has become larger. Moreover, when comparing the results from the two levels of theory used, MP2 yields a more delocalized distribution of the charge than SCF does. Therefore, when electron correlation is included we get a better description of the three-center two-electron bond, which translates into a larger stabilization of TS, that can explain the aforementioned decrease of the energy barrier.

These results reflect (a) the significant difference in character between H_t and the other terminal hydrogen atoms, and (b) the large ability of the transferring-H to transport the residual electron density of the initially bonded H_3C fragment to the other CH_3 fragment. Thus, this outcome gives support to the postulated inner-sphere electron transfer mechanism.

Since the way how electron density is apportioned to atoms is arbitrary, atomic charges are usually defined inexactly. On the contrary, the total electron density is a quantum-mechanical observable, so the next step in this electronic analysis will be to construct isodensity contour maps, together with an analysis of the gradient and laplacian of this electron density. Such an information has been thoroughly and skilfully exploited by Bader [13].

In Fig. 2 we have portrayed the two density contour maps of the reactant complex (2a) and the transition state (2b) at the SCF level, in a plane containing the three atoms involved in the transfer process and two staggered terminal hydrogens. In the RC density map (2a) H_t is still bonded to the CH_3^{ℓ}, the C^{ℓ}–H_t bond critical point (BCP^{ℓ}) being lower than the terminal C–H BCP. This indicates the fact that H_t just begins to be transferred. If we consider H_t to be at the origin of the coordinates, BCP^{ℓ} is located at 0.484 Å from H_t to C^{ℓ} with a density value of 0.239 a.u. The density value on top of H_t is 0.428 a.u. The H_t–C^r interaction is revealed by the bond critical point at 0.980 Å from H_t to C^r with a density value of 0.017 a.u. In TS density map (2b), H_t has been displaced to the midpoint of the C–C distance. The density value on top of H_t is now 0.382 a.u. (significantly lower than at RC). Besides, a small amount of electron density between both C–H_t bonds can be envisaged. The two symmetric bond critical points are located at 0.690 Å from H_t with a density value of 0.075 a.u. This supplies a first idea of the delocalized character of the C–H_t–C three-center two-electron bond.

From a Bader analysis, the laplacian distribution recovers the electronic shell model of an atom by exhibiting a corresponding number of pairs of shells of charge concentration and charge depletion, in such a way that it has become a quite useful tool in characterizing atomic interactions. Thus, to gain a deeper insight in this aspect, we have depicted in Fig. 3 the contour map of the laplacian of the charge

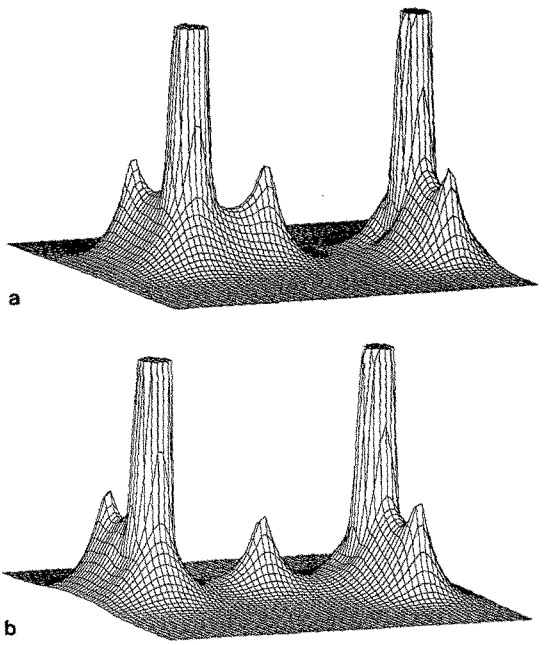

Fig. 2a, b. Three-dimensional charge density maps of the reactant complex (**a**) and transition state (**b**) at the SCF level.

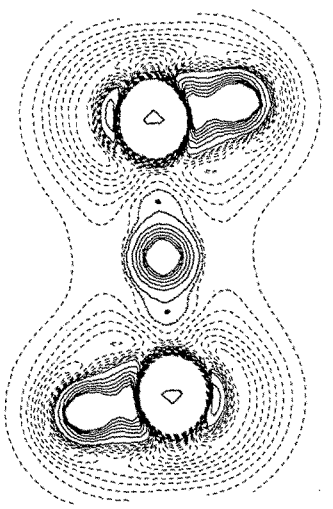

Fig. 3. Laplacian of the charge density contour map for the transition state at the SCF level. Solid lines stand for negative values, dashed lines for positive values, and the dot-dashed line indicates the zero-value line. Bond critical points are marked with a dot.

density for the transition state at the SCF level. Negative values of the laplacian i.e., regions where electronic charge is concentrated, are given by the solid contours, while positive values, i.e., the regions where electronic charge is depleted, are represented by the dashed lines. It is clear from this illustration that negative values are obtained around H_t. Moreover, one can observe that the *s* shell of H_t has been clearly distorted and oriented towards carbons. Such a shape might be well related

to the formation of a three-center two-electron bond. Special attention deserve bond critical points, which have been marked with a dot. At such points, negative values of the laplacian of the charge density have been found (−0.030 a.u.). In practice, we have searched for laplacian values until the change in sign is produced: the change has been located at 0.864 Å from H_t. Although the laplacian figure for RC is not presented, we have also found a clear negative value on BCP^{ℓ} (−0.725 a.u.) and a small positive value on BCP^{r} (0.051 a.u.). From these values it is quite possible to say that, from a Bader language, the C^{ℓ}–H_t bond has a clear covalent character, while H_t presents an ionic interaction with C^{r}.

The fact that at the BCP of TS a small negative value of the laplacian has been found, indicates that a bond with some covalent character is achieved between both carbon atoms and H_t. This information gives support again to a possible inner-sphere electron transfer mechanism, and excludes a clear direct hydride mechanism, which would imply that positive values of the laplacian be found at the BCP to embody ionic interactions. Furthermore, from the results obtained for the natural bond orbital analysis, one can expect that when electron correlation be included, the covalent character of both C–H_t bonds will be reinforced because three-center two-electron bond becomes more delocalized.

A final comment in this section concerns the gradient contour map of the transition state at the SCF level, rendered at Fig. 4. This type of map may be used to establish the atomic basins to compute the atomic charges from a point of view of a Bader analysis [13]: he has shown that the zero-flux surfaces are natural boundaries with many useful properties. This procedure for computing atomic charges has been recently criticized [15] in terms of electronegativity differences and atomic-size dependence. Furthermore, calculation of this type of charges supposes a great computational effort and, for this reason, will not be considered here. Another interesting feature of this kind of figures is that bond critical points can be clearly located. In this aspect, the information obtained from this picture confirms the conclusions obtained from the density map (Fig. 2b).

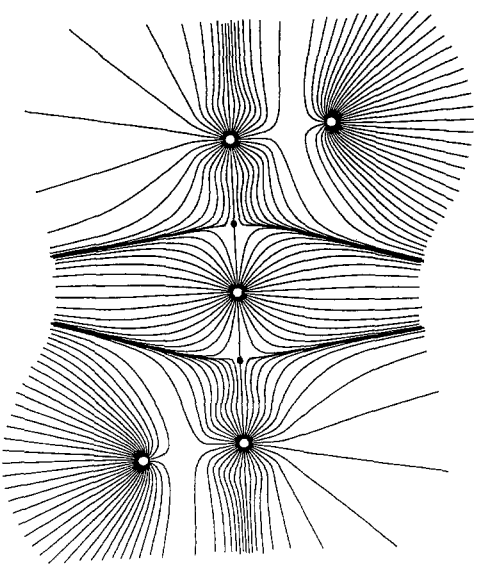

Fig. 4. Density flux map for the transition state (D_{3d} symmetry) at the SCF level. Bond critical points are marked with a dot.

3.2 Effect of a uniform electric field

A practical way to simulate the environment of chemical processes is by application of a uniform electric field, supported by the well-known experimental fact that the presence of an electric field can dramatically change the rate of chemical processes. In the present work, a uniform electric field has been applied to model, in some manner, the electric field created by the proteinic environment in the active site of the enzyme where the hydride transfer process takes place.

This uniform electric field has been suitably applied along the C–H_t–C axis to promote the transfer of H. The buildup of the perturbed potential energy profile has been accomplished by applying the field on each point of the field-free reaction coordinate. As shown recently in our group [16], this procedure gives results analogous to those obtainable through reoptimization of geometries. This method can be used here because the uniform electric field can be applied in the same direction as the reaction coordinate. All in all, expensive calculation of real perturbed potential energy profiles can be avoided.

In Table 5 we have collected the geometrical parameters, as defined in Scheme I, together with the SCF absolute energies and relative energies with respect to the reactant complex, when a uniform electric field of 0.005 a.u. has been applied. Comparing these results with those obtained for the gas-phase reaction (Table 1) one can notice several meaningful changes. First, application of the field leads the symmetry of the process to break down completely. This fact can be noted both from the geometrical parameters and from the energy values. In this case, relative to the gas phase, $r1$ in RC has been lengthened from 1.1240 to 1.1597 Å, thus showing that the H-transfer event has been favoured by application of this uniform electric field. Moreover, now $r2$ in PC (1.1015 Å) has no longer the same value that $r1$ in RC (1.1597 Å), reflecting the distortion of the process. If we define the reaction coordinate, q, as the difference between $r1$ and $r2$, RC and PC are found later along the reaction coordinate, comparing with the gas-phase process ($\Delta q = +0.0714$ and $\Delta q = +0.0450$ Å, respectively). Looking at the TS, it can be appreciated that now this point is reached earlier than in the gas-phase reaction (if one takes as a reference $q = 0.0$ Å for TS in the gas-phase reaction, now TS is located at $q = -0.2$ Å).

The distortion in the symmetry of the process is also perceived watching the perturbed energy values: while RC has suffered an energy destabilization with respect to RC in the gas-phase reaction, PC has been strongly stabilized and, hence, the TS is advanced along the reaction coordinate, in agreement with Hammond's postulate [17]. Here the effect of the uniform electric field in the process can be pondered, since the forward energy barrier has been reduced from 13.68 kcal/mol in the gas-phase reaction to 5.20 kcal/mol when a uniform electric field of 0.005 a.u.

Table 5. Geometrical parameters (in Å), energies (in hartrees) and energy barriers (in kcal/mol) for the reactant complex, the transition state and the product complex at the SCF level, when a uniform electric field of 0.005 a.u. is applied

Point	$r1$	$r2$	$a1$	$a2$	E	ΔE
RC	1.1597	2.0403	106.66	91.32	−79.43304	0.00
TS	1.5	1.7	99.34	95.86	−79.42475	5.20
PC	2.0985	1.1015	91.22	107.81	−79.46397	−19.20

has been applied. The limit value of the uniform electric field, i.e., the strength of the uniform electric field beyond which there is no longer an energy barrier, has been found for ca. 0.01 a.u. (where the energy barrier is 0.2 kcal/mol). These data indicate the large sensitivity of this kind of process to environmental effects, since the energy barrier disappears when a moderate electric field is applied.

A fundamental point in enzymic catalyses is the reversibility of the process. In a limit case, the most efficient catalyzed enzymic reaction should have both forward and reverse ways with the same energy barrier. Up to now, we have shown how a uniform electric field can modify the energetic barriers of a given process: in the system studied in this work, the gas-phase potential energy profile is completely symmetric, and application of the uniform electric field breaks down this symmetry, diminishing the forward barrier and increasing the reverse; thus, in this case, application of the electric field is against the reversibility of the process. However, general hydride transfers usually occur between donor and acceptor species involving different heteroatoms, the potential energy profile not being symmetric at all. Then, in such cases, we could apply an electric field in the way that the reversibility of the process will be favoured, and then efficiently catalyzing the reaction.

In Table 6 we have collected the values obtained from an MPA. Comparing these results with those obtained for the gas-phase reaction (Table 2), one can scrutinize several interesting changes: (a) the charge of H_t in RC becomes more negative when the uniform electric field is applied in a suitable fashion to favor the hydride transfer, as a consequence of the displacement of the electronic cloud. For the same reason, the charge on CH_3^{ℓ} becomes more positive and the charge on CH_3^{r} becomes less positive. Thus, a small amount of charge transfer at RC is found; (b) the charge on H_t in TS is practically the same than in the gas phase, but the charge on CH_3^{ℓ} is slightly less positive, and on CH_3^{r} slightly more positive; (c) all charges on the three fragments in PC suffer an effect inverse to that suffered in RC.

The consequences of these aspects are very important. We have recomputed the fragment charges in the gas phase at $q = -0.2$ Å (within parentheses in Table 6). From these values, it is interesting to check that the charge on H_t does not change, thus showing that H_t acts roughly as a simple charge transporter. Moreover, the charge on CH_3^{r} in the gas phase is more positive than when the uniform electric field is applied, reflecting that the charge transfer is less favoured in the gas phase reaction at the same point along the reaction coordinate than in the case perturbed in the correct way to favor the H-transfer event.

Table 6. Mulliken population analysis using the SCF density matrix, when a uniform electric field of 0.005 a.u. is applied. In TS column we have added, in parenthesis, the fragment charge values at the same point of the rection coordinate ($q = -0.2$ Å) for the gas-phase reaction.

Fragment	RC	TS	PC	ΔQ
H_t	−0.1204	−0.1799 (−0.1799)	−0.0576	−0.0595
CH_3^{ℓ}	0.2303	0.5406 (0.5371)	0.9398	0.3103
CH_3^{r}	0.8901	0.6393 (0.6428)	0.1178	−0.2508
Q_{trans}	−0.1099	−0.3607	−0.8822	−0.7723

Regarding the influence of the electric field on Figs. 1a and 1b, results arising from our calculations lead to meaningless differences when the field is included, so conclusions similar to the gas phase can be drawn. As to plots involving the charge density, the same argument and the little influence of the field on H_t population suggest slight changes in bond critical points positions and values, for the same point along the reaction coordinate.

Furthermore, looking at Table 6, if we divide ΔQ undergone by CH_3^r by the total Q_{trans} of the process, we obtain that, now, a 32.47% of the charge has been transferred at TS while in the gas-phase case a 44.07% has already been transferred. This arises from the fact that the TS point is reached earlier with the application of the electric field. Thus, although we have checked that when a uniform electric field is applied the charge transfer event is favoured, in the TS there is less percentage of charge transfer.

Nevertheless, one could regard the process in the reverse way. In this case, TS would be found at $q = +0.2$ Å, the reverse energy barrier would be increased to 24.61 kcal/mol, and the percentage of charge transfer would become 67.53%; thus, now, with respect to the gas-phase process, the charge transfer would be less favoured. This result is consistent with earlier results obtained by Tapia et al. [6(b), 6(d)] where a reaction field is applied in such a way that the transition state is reached later than in gas phase.

4 Conclusions

In our earlier preliminary work on this subject [7], where the hydride transfer event on the $[CH_3–H–CH_3]^+$ system was studied in terms of valence bond structures, we arrived to the conclusion that, although the multistep electron transfer mechanism could not be totally rejected, the one-step formal direct hydride transfer had the large probability. However, all calculations were accomplished with a minimal basis set at SCF level. At that stage, ionic structures were largely exaggerated. Improving of the basis set and inclusion of electron correlation would correct this defect and would bring down the exaggerated weight of the direct hydride transfer mechanism.

From our present results we can conclude first, that the H atom to be transferred has only a weak negative charge at all levels of theory used; second, that at the TS point, negative values of the laplacian of the charge density on the bond critical points are found at the SCF level, thus showing the formation of a three-center two-electron bond that becomes more delocalized when electron correlation is included; third, that when a uniform electric field is applied in a way to favor the H-transfer event (i.e., to reduce the forward energy barrier), the charge transfer is more favoured than when the process takes place in the gas phase; however, if it is applied in the reverse way the charge is less favoured. It is interesting to remark that in both cases the charge on the H being transferred, at the transition state, remains practically invariant upon perturbation by a field with respect to the gas-phase process. In this sense, both in the gas phase and when a uniform electric field is applied, the motion of the H atom and the charge transfer are coupled, i.e., an inner-sphere electron transfer mechanism takes place. As regards to this coupling, the central hydrogen acts as a charge transporter, and for that reason these kinds of processes can be referred to as formal hydride transfers. More research in the so-called formal hydride transfer processes is in progress in our laboratory.

Acknowledgements. Financial help has been provided by the Spanish "Dirección General de Investigación Científica y Técnica" under project No. PB89-0318. J.M. acknowledges the financial help provided by the Generalitat de Catalunya through CIRIT Project No. AR91-425.

References

1. Mauzerall D, Westheimen FH (1955) J Am Chem Soc 77:2261
2. (a) Bunting JW, Sindhuatmadja S (1981) J Org Chem 46:4211; (b) Bunting JW, Chew VSF, Chu G (1982) J Org Chem 47:2303; (c) Bunting JW (1991) Bioorg Chem 19:456
3. (a) Ostović D, Roberts RMG, Kreevoy MM (1983) J Am Chem Soc 105:7629; (b) Kreevoy MM, Lee I-SH (1984) J Am Chem Soc 106:2550; (c) Kreevoy MM, Ostović D, Truhlar DG, Garrett BC (1986) J Phys Chem 90:3766; (d) Kreevoy MM, Ostović D, Lee I-SH, Binder DA, King GW (1988) J Am Chem Soc 110:524; (e) Lee I-SH, Ostović D, Kreevoy MM (1988) J Am Chem Soc 110:3989; (f) Kim Y, Truhlar DG, Kreevoy MM (1991) J Am Chem Soc 113:7837; (g) Kotchevar AT, Kreevoy MM (1991) J Phys Chem 95:10345
4. (a) van Bergen TJ, Kellogg RM (1977) J Am Chem Soc 99:3882; (b) van der Veen RH, Kellogg RM, Vos A, van Bergen TJ (1978) JCS Chem Comm 923; (c) de Vries JG, Kellogg RM (1979) J Am Chem Soc 101:2759; (d) Piepers O, Kellogg RM (1980) JCS Chem Comm 1154; (e) Kellogg RM, van Bergen TJ, van Doren H, Hedstrand D, Kooi J, Kruizinga WH, Troostwijk CB (1983) J Org Chem 45:2854; (f) Mashraqui SH, Kellogg RM (1983) J Am Chem Soc 105:7792; (g) Kellogg RM (1984) Angew Chem Int Ed Engl 23:782
5. Dewar MJS, Storch DM (1985) Proc Natl Acad Sci USA (Biochemistry) 82:2225
6. (a) Tapia O, Andrés J, Aullo JM, Bränden C-I (1985) J Chem Phys 83:4673; (b) Tapia O, Andrés J, Aullo JM, Cardenas R (1988) J Mol Struct (Theochem) 167:395; (c) Tapia O, Cardenas R, Andrés J, Colonna-Cesari F (1988) J Am Chem Soc 110:4046; (d) Tapia O, Cardenas R, Andrés J, Krechl J, Campillo M, Colonna-Cesari F (1991) Int J Quantum Chem 39:767; (e) Tapia O, Andrés J, Cardenas R (1992) Chem Phys Lett 189:395
7. Mestres J, Lledós A, Duran M, Betrán (1992) J Mol Struct (Theochem) 260:259
8. Yadav A, Jackson RM, Holbrook JJ, Warshel A (1991) J Am Chem Soc 113:4800
9. Hariharan PC, Pople JA (1973) Theor Chim Acta 28:213
10. (a) Schlegel HB (1982) J Comp Chem 3:214; (b) Schlegel HB (1984) Theor Chim Acta 66:333
11. Reed AE, Weinstock RB, Weinhold F (1985) J Chem Phys 83:735
12. Gaussian 90. Frisch MJ, Head-Gordon M, Trucks GW, Foresman JB, Schlegel HB, Raghavachary K, Robb MA, Binkley JS, González C, Defrees DJ, Fox DJ, Whiteside RA, Seeger R, Melius CF, Baker J, Martin RL, Kahn LR, Stewart JJP, Topiol S, Pople JA, Gaussian, Inc., Pittsburg, PA, 1990.
13. (a) Gatti C, MacDouglas PJ, Bader RFW (1988) J Chem Phys 88:3792; (b) Bader RFW (1991) Chem Rev 91:893
14. Sustmann R, Sicking W, Schulz GE (1989) Angew Chem Int Ed Engl 28:1023
15. Perrin CL (1991) J Am Chem Soc 113:2865
16. Mestres J, Duran M (1993) Int J Quantum Chem 47:307
17. Hammond GS (1955) J Am Chem Soc 77:334